International Journal of Fatigue 33 (2011) 1539–1547

Contents lists available at ScienceDirect

International Journal of Fatigue

journal homepage: www.elsevier.com/locate/ijfatigue

Corrosion fatigue behaviour of aluminium alloy 6061-T651 welded using fully automatic gas metal arc welding and ER5183 filler alloy

Kalenda Mutombo [a,*], Madeleine du Toit [b]

[a] CSIR, Materials Science and Manufacturing, PO Box 395, Pretoria 0001, South Africa
[b] University of Pretoria, Materials Science and Metallurgical Engineering, Pretoria 0002, South Africa

ARTICLE INFO

Article history:
Received 19 January 2011
Received in revised form 14 June 2011
Accepted 17 June 2011
Available online 13 July 2011

Keywords:
6061-T651 aluminium alloy
Pulsed gas metal arc welding
ER5183 filler wire
Pitting corrosion
Corrosion fatigue properties

ABSTRACT

The fatigue life of aluminium 6061-T651 at various applied stress amplitudes in the unwelded and welded condition was found to be significantly reduced on immersion in a 3.5% NaCl simulated sea water solution, compared to that measured in ambient air. The ratio of fatigue life in NaCl test solution to that in air increased as the stress amplitude decreased. The observed reduction in the fatigue life in the NaCl test solution was most likely due to the presence of pits which nucleated on second phase particles or precipitates. Welded joints performed using pulsed gas metal arc welding and ER5183 filler wire failed at the interface between the weld metal and the heat-affected zone as a result of a high pitting rate in this region.

1. Introduction

Artificially aged 6061-T651 aluminium alloyed with magnesium and silicon displays high strength, excellent extrudability, reasonable weldability and good corrosion resistance. This alloy finds widespread application in ship building (civil and military) and in the fabrication of tank containers for transporting various liquids, where is often welded during manufacturing process. Artificially aged 6061-T651 aluminium alloyed with magnesium and silicon displays high strength, excellent extrudability, reasonable weldability and good corrosion resistance. This alloy finds widespread application in ship building (civil and military) and in the fabrication of tank containers for transporting various liquids, where is often welded during manufacturing process. However welded joints of heat treatable aluminium alloys displayed a significant reduction in hardness, and mechanical properties. The friction stir-welded joint of 2024-T4 has displayed reduced hardness and tensile strength, as observed by Aydin et al. [1]. Elangovan and Balasubramanian observed also inferior tensile properties in AA6061 welded joints after friction stir-welding [2]. Similarly the tensile properties and the fatigue properties were sensibly reduced after pulsed gas tungsten arc welding (GTAW) process and pulsed gas metal arc welding (GMAW) process of AA7075 aluminium alloy, as observed by Balasubramanian et al. [3,4]. These welds failed in the soft and overaged heat-affected zone resulted from welding process.

Aluminium 6061-T651 is, additionally, prone to pitting corrosion in chloride-containing environments. The aluminium-rich matrix adjacent to $MgSi_2$ intermetallic precipitates or silicon-rich phases in aluminium–silicon–magnesium alloys has been shown to be susceptible to preferential corrosion in NaCl solutions [5]. Guillaumin and Mankowski observed that coarse intermetallic particles containing aluminium, silicon and magnesium act as nucleation sites for pit formation [6]. The formation of pits, in turn, has a detrimental effect on the fatigue life of 6061 aluminium. The fatigue life of aluminium alloys has been shown to be significantly reduced when tested in a 3.5% NaCl solution compared to the fatigue life of the same alloy in air. This reduction in fatigue life has been attributed to premature crack initiation from surface pits by Chlistovsky et al. [7], Rebiere and Magnin [8] and Rokhlin et al. [9], and higher crack growth rate resulting from synergistic interaction of fatigue and stress corrosion as observed by Maeng et al. [10].

Although the fatigue behaviour of aluminium alloy 6061 has been studied in depth, its behaviour when simultaneously subjected to a corrosive environment consisting of simulated sea water (or a 3.5% NaCl solution) and constant amplitude fatigue loading in the welded condition is not well understood. This investigation studied the corrosion fatigue behaviour of aluminium 6061 in the T651 temper condition, and determined the corrosion damage ratio (ratio of the fatigue life in a NaCl solution to the fatigue life in air). The influence of welding using magnesium-alloyed ER5183 aluminium filler wire and fully automatic pulsed gas metal arc welding (GMAW-P) on the fatigue life of 6061-T651 aluminium in air and in a NaCl solution was also measured in this investigation.

* Corresponding author. Tel.: +27 784363580; fax: +27 128413378.
E-mail address: kmutombo@csir.co.za (K. Mutombo).

0142-1123/$ - see front matter © 2011 Elsevier Ltd. All rights reserved.
doi:10.1016/j.ijfatigue.2011.06.012

2. Experimental procedure

Plates of aluminium alloy 6061 in the T651 temper condition (with initial dimensions of 2000 mm long, 120 mm wide and 6.35 mm thick) and a chemical composition shown in Table 1 were joined using fully automatic pulsed gas metal arc welding and non-matching ER5183 (Al–Mg) filler wire (see Table 1 for the nominal chemical composition of ER5183). ER5183 is a popular filler metal for welding alloy 6061 due to its high resistance to solidification cracking during welding. Pulsed gas metal arc welding was used to ensure adequate fusion while limiting the heat input into the base metal. The plates were sectioned, degreased and welded with a square edge joint preparation, as shown in Fig. 1a, using the welding parameters given in Table 2.

The welded and unwelded plates were sectioned and machined to produce rectangular fatigue test specimens with the dimensions shown in Fig. 1b. Metallographic samples were prepared in both the longitudinal and transverse directions, as shown in Fig. 1a, according to the requirements of ASTM standard E3-01 [11] for microstructural analysis. These sections were etched using the modified Keller's reagent as prescribed in ASTM standard E340 [12] and examined using an optical microscope and a scanning electron microscope (SEM) equipped to perform energy dispersive X-ray spectroscopy (EDS analysis).

The machined fatigue specimens were ground flush and polished in the longitudinal direction to dress the welds and to remove all machining marks from the unwelded samples. This negated the effect of the weld geometry on the fatigue resistance of the welded samples, as shown by Mutombo and Du Toit in their previous investigation [13].

Vickers Microhardness tests were performed on as polished samples, according to the ASTM standard E92 [14]. A loading of 10 gf and a dwell time of 10 s were set on the Vickers Microhardness Tester FM-700 equipped with HDPS-ARC ver.1.23 software. Hardness profiles from the fusion centre line of the weld metal (WM), through the heat-affected-zone (HAZ), to the base metal (BM) (dot lines, Fig. 3c) were constructed for welded and unwelded specimens.

The fatigue tests were performed using a symmetric tension–tension cycle (with a stress ratio $R = 0.125$) to keep the crack open during testing. A constant frequency of 1 Hz was used for all fatigue tests and the number of cycles to failure was recorded for each specimen. Between three and six tests were performed at each stress level depending on the quality of the weld, as recommended by ASTM standard E466 [15]. The fatigue tests in ambient air were

Table 1
Chemical composition of the aluminium 6061-T651 plate material and the nominal composition of the ER5183 filler wire used in this investigation (percentage by mass).

Element (%)	Al	Mg	Mn	Fe	Si	Cr	Cu	Zn	Ti	Others total
6061-T651	Balance	0.96	0.09	0.40	0.80	0.21	0.27	0.00	0.02	<0.01
ER5183	Balance	5.00	0.80	<0.40	<0.4	<0.1	<0.1	<0.25	<0.15	<0.15

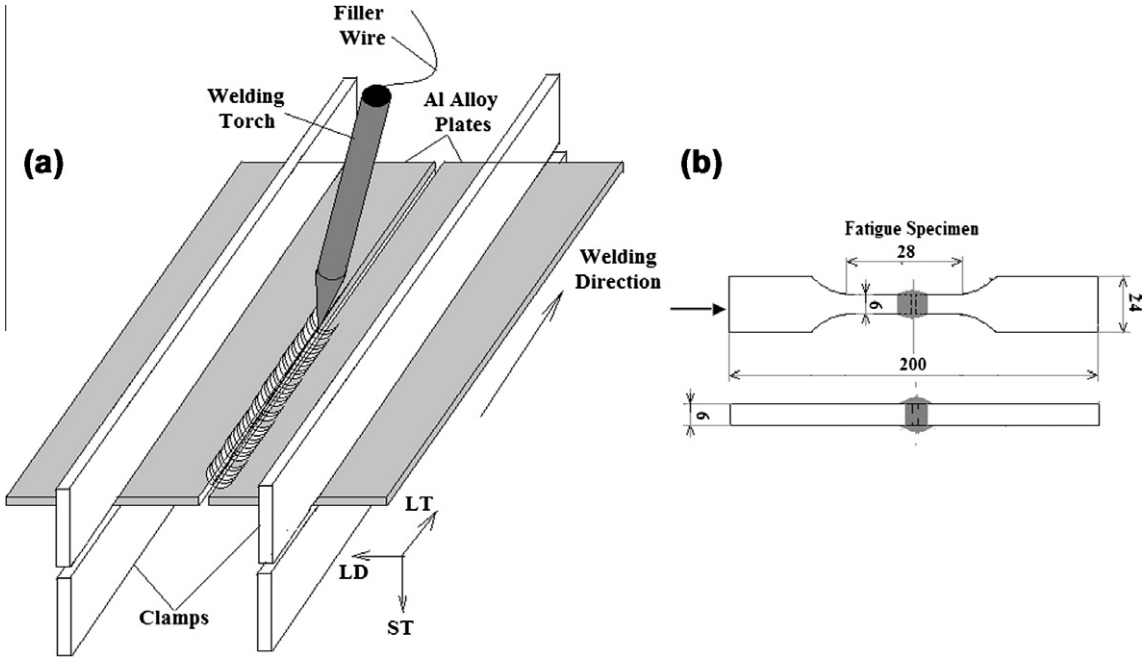

Fig. 1. (a) Schematic illustration of the experimental set-up during welding; and (b) fatigue specimen preparation (dimensions in mm).

Table 2
Pulsed gas metal arc welding process parameters.

Parameters Unit	Arc voltage V	Welding current A	Wire feed speed m/min	Wire diameter mm	Nozzle to plate distance mm	Travel speed m/min	Torch angle °	Gas flow rate l/min
	20–23	133–148	6.1–7.6	1.2–1.6	15–20	0.4–0.6	60–80	19–28

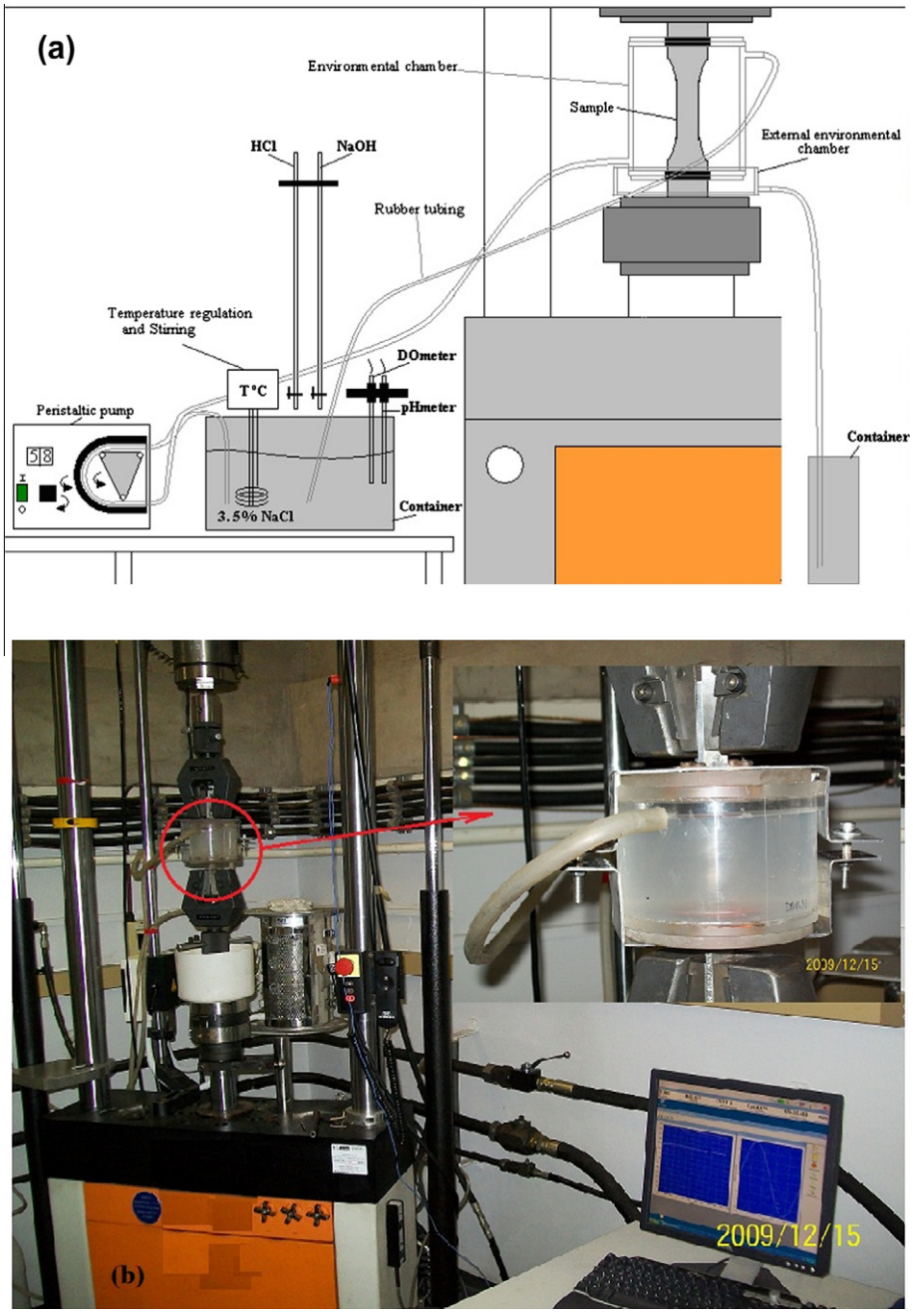

Fig. 2. (a) Schematic illustration of the experimental set-up for corrosion fatigue testing in 3.5% NaCl; and (b) Plexiglas corrosion fatigue chamber on the tensile testing machine.

performed at temperatures ranging between 19 °C and 20 °C and at relative humidity levels between 35.7% and 70.6% RH (relative humidity). INSTRON™ testing machines, equipped with calibrated load transducers, data recording systems and FASTTRACK™ software, were used to fatigue specimens to failure under amplitude stress control, as required by ASTM standard E467 [16]. Welded specimens were inspected before testing and any specimens with visual welding defects, such as large pores, underfill, excessive undercut or craters, were discarded. The fatigue specimens were cleaned with ethyl alcohol prior to testing to remove any surface oil, grease and fingerprints.

A corrosion environment consisting of 3.5% NaCl (by weight) in distilled water was used with the axial fatigue life testing method to investigate the effect of pitting corrosion on fatigue life. The corrosion chamber was designed and manufactured from Plexiglas, as shown in Fig. 2a and b. The NaCl solution was re-circulated from 25 litre storage containers at a constant flow rate by means of a peristaltic pump. The dissolved oxygen (DO) content, NaCl solution flow rate, pH, temperature, stress amplitude (maximum and minimum stress) and frequency were controlled, as shown in Fig. 2a. The measured DO content varied between 7 and 8 ppm (parts per million) during testing. The number of cycles to failure (N_f) was recorded for each stress amplitude (S) at the end of the test.

Following testing, the S–N_f curve (represented as stress–log N_f) was determined from the average number of cycles to failure at each stress level. In order to compare the fatigue resistance in air to that in NaCl, the damage ratio, which is the ratio of the fatigue life in the 3.5% NaCl solution to the fatigue life in air

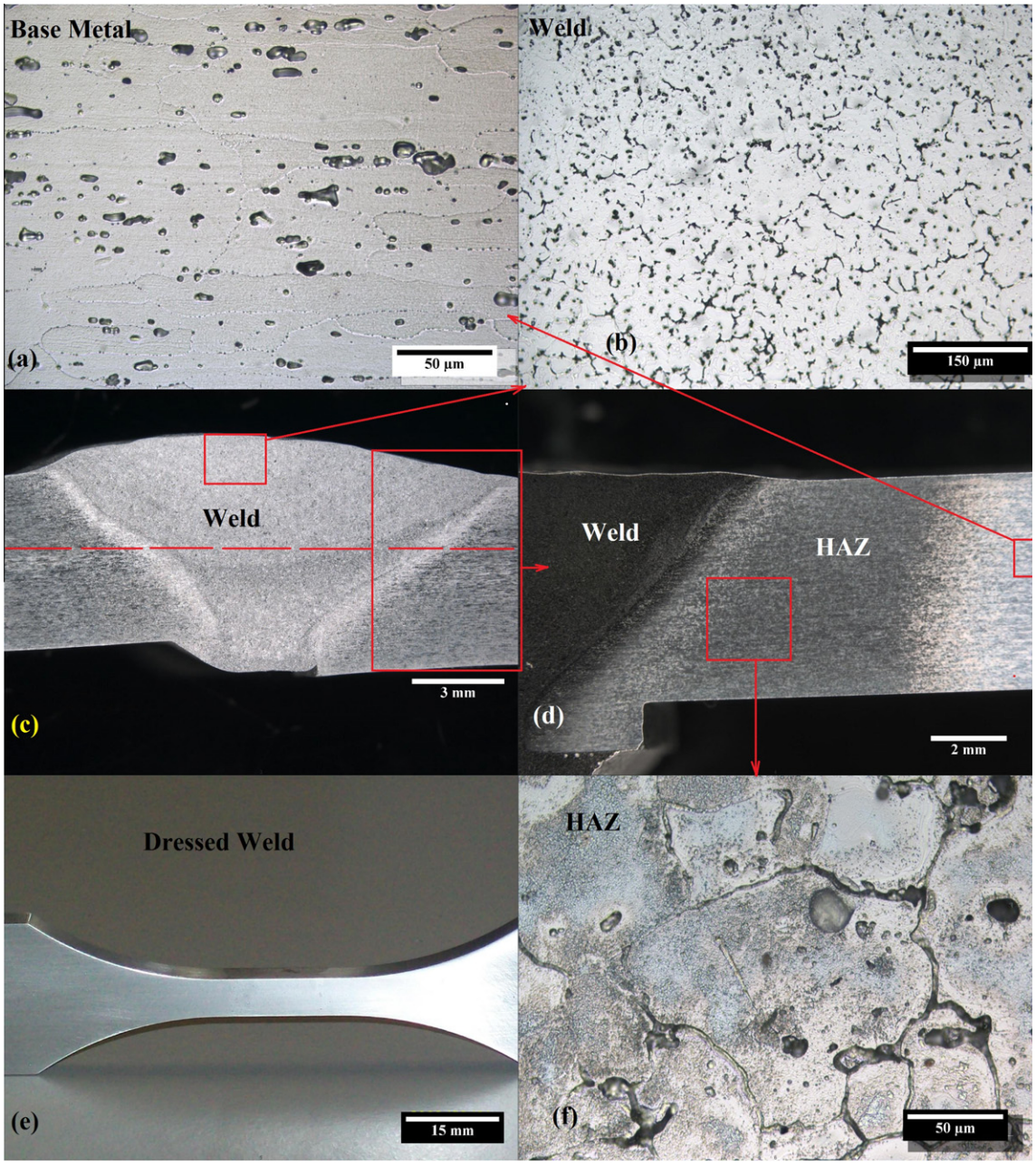

Fig. 3. (a) Optical micrograph of the 6061-T651 aluminium base metal microstructure; (b) optical micrograph of the 6061/ER5183 weld metal microstructure; (c) and (d) macrographs of the 6061/ER5183 welds; (e) dressed fatigue specimen of a 6061/ER5183 weld; and (f) HAZ microstructure.

($N_{f\ NaCl}/N_{f\ Air}$), was calculated and presented as a curve of stress amplitude against $N_{f\ NaCl}/N_{f\ Air}$.

3. Results and discussion

The variation in microstructure across the welded joint is shown in Fig. 3a–f. Microstructural analysis revealed a coarse, elongated grain structure in the 6061-T651 base metal, as shown in Fig. 3a, with average grain dimensions of 141.1 μm in length (standard deviation of 70.3 μm) and 29.2 μm in width (standard deviation of 17.5 μm). Coarse second-phase particles and fine grain boundary precipitates are evident. The heat-affected zone (HAZ) adjacent to the weld fusion line consists of coarse, equiaxed grains with an average grain diameter of 100.0 μm (standard deviation of 42.5 μm) (Fig. 3f). A grain boundary film of second-phase particles, signifying uncontrolled precipitation during the weld thermal cycle, is evident in Fig. 3f. The weld metal microstructure is more dendritic in appearance with an average grain size of 107.2 μm (standard deviation of 36.7 μm) and exhibits some evidence of interdendritic second-phase particles (Fig. 3b).

Heterogeneous structure and high degree of HAZ softening had been noticed in Al6061/ER5183 joint, as shown by the microhardness profile (Fig. 4). The low hardness observed in the heat-affected zone is due to the partial dissolution, overaging and uncontrolled reprecipitation of strengthening precipitates during the weld thermal cycle.

The experimentally determined *S–N* curves for the unwelded 6061-T651 base metal and the polished 6061/ER5183 gas metal arc welds, tested in air and in a NaCl solution, are shown in Fig. 5. Each data point represents the average of between three

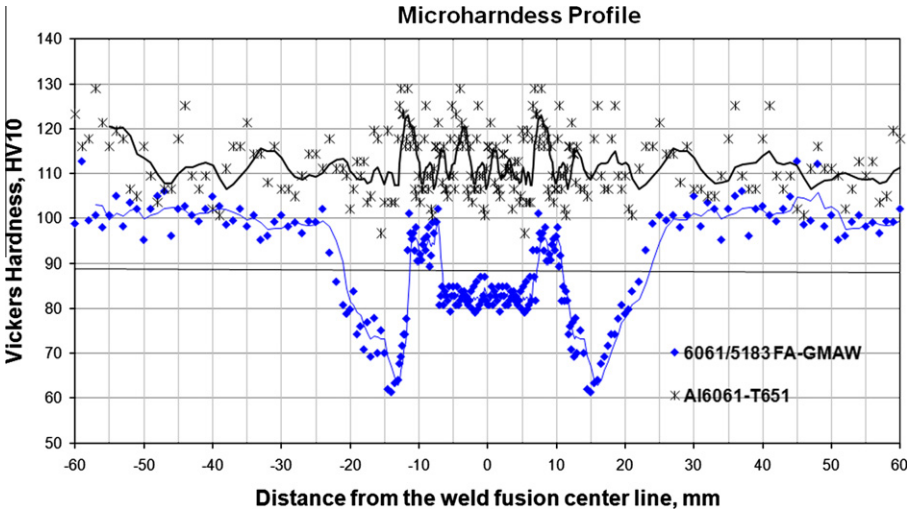

Fig. 4. Microhardness profile of 6061/5183 FA-GMAW and aluminium alloy 6061-T651.

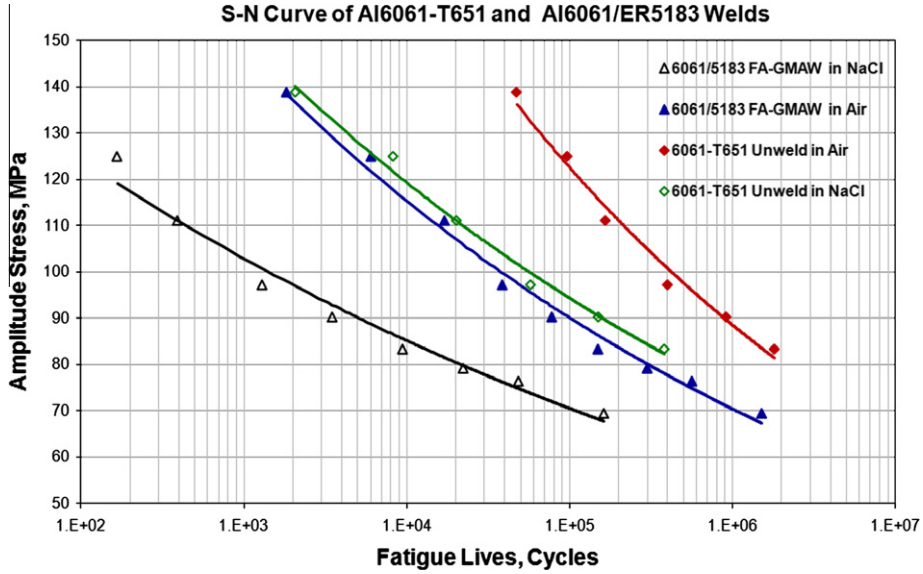

Fig. 5. Fatigue *S–N* curves of aluminium 6061-T651 and 6061/ER5183 welds tested to failure in ambient air and in a 3.5% NaCl solution.

and six tests performed at a given stress amplitude. Unwelded 6061-T651 aluminium tested in the ambient atmosphere displayed the highest fatigue properties of the samples tested, with an allowable stress amplitude of 90 MPa for an average fatigue life of 1×10^6 cycles to failure. Continuous immersion in a NaCl solution reduced the allowable stress amplitude to well below 80 MPa for an average fatigue life of 1×10^6 cycles to failure. Welded 6061/ER5183 samples, tested in air, displayed fatigue properties slightly below those of unwelded samples tested in NaCl, with an allowable stress amplitude of approximately 70 MPa for an average fatigue life of 1×10^6 cycles to failure. The fatigue performance of welded 6061/ER5183 samples was, however, reduced significantly on testing in a NaCl solution, with the welded samples failing prematurely at much reduced stress amplitudes.

To explain the differences in fatigue performance of the various samples, the fracture surfaces were examined optically and using a scanning electron microscope (SEM). The crack location in unwelded aluminium 6061-T651 tested in ambient air is shown in Fig. 6a, and the fracture surface in Fig. 6b. Multiple fatigue cracks apparently initiated at the free surface of the sample, with one crack propagating to failure during testing. Crack initiation apparently occurred as result of the interaction between slip lines and intermetallic particles or inclusions, as shown in Fig. 6b, with precipitates acting as microscopic surface stress raisers and preferential crack initiation sites. As shown in Fig. 5, fatigue failure of unwelded aluminium 6061-T651 was accelerated by immersing the samples in a 3.5% NaCl solution. The location of the crack and the specimen surface in the vicinity of the fatigue crack are shown in Fig. 7a–d. Examination of the fracture surface suggests that the fatigue life reduction in NaCl can be attributed to rapid fatigue crack initiation from corrosion pits (as illustrated in Fig. 7c and d). These pits act as stress raisers and seem to be associated with precipitates within the 6061-T651 aluminium matrix (Fig. 7b and d).

As shown in Fig. 8a and b, fatigue failure of 6061/ER5183 welded samples in ambient air occurred in the heat-affected zone adjacent to the fusion line of the weld. Fatigue cracks apparently initiated at coarse precipitates or inclusions, as illustrated in

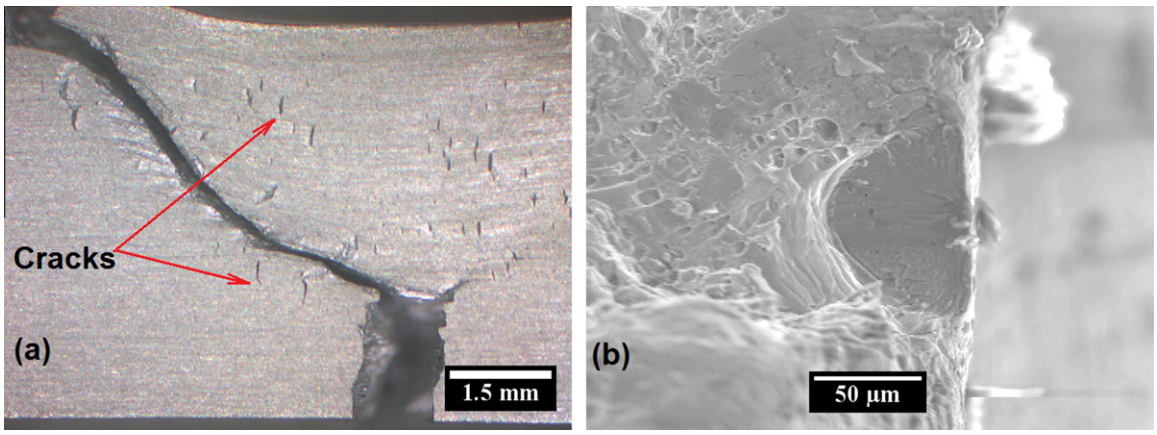

Fig. 6. Fatigue failure of unwelded aluminium 6061-T651 in air: (a) cracks on the free surface; and (b) the crack initiation site.

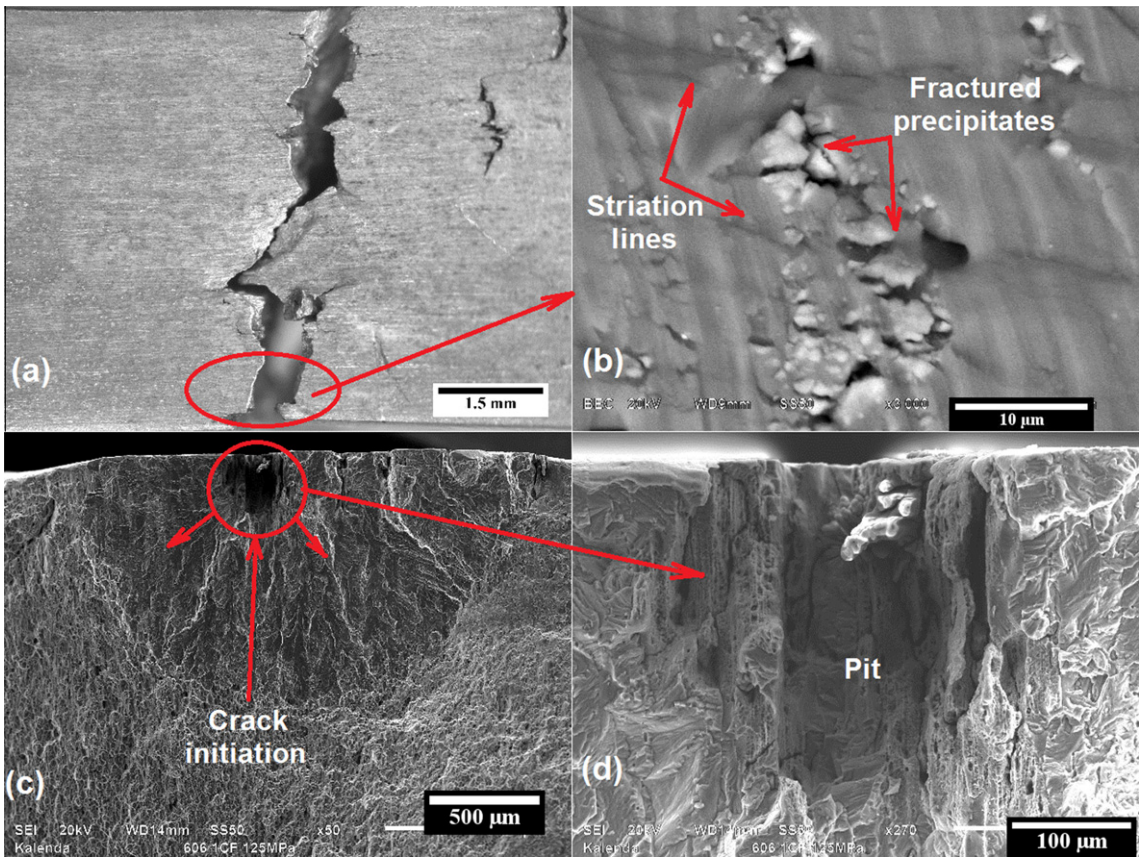

Fig. 7. Failure of unwelded aluminium 6061-T651 in a 3.5% NaCl solution: (a) crack location; (b) corrosion pits associated with fractured precipitates on the fracture surface; (c) the fatigue crack initiation site; and (d) a corrosion pit at the crack initiation site.

Fig. 8c, and propagated preferentially within the heat-affected zone. During fracture, coarse precipitates were pulled out of the heat-affected zone matrix.

The observation that failure occurred preferentially in the heat-affected zone is consistent with coarse equiaxed grains formation, phase particle dissolution (leading to free precipitate zone and lower dislocation density) because of the prevailing thermal conditions during welding process and weld metal solidification. Most of the deformation is concentrated in the soft heat-affected zone region, protecting the weld metal, but resulting in premature failure adjacent to the weld. Since failure occurs preferentially in the heat-affected zone, filler metal selection and welding technique have less influence on the fatigue properties of welded joints in 6061-T651 aluminium.

Fatigue failure of the 6061/ER5183 weld tested in a 3.5% NaCl solution occurred within the coarse grained region of the heat-affected zone at the weld fusion line, as shown in Fig. 9a. Preferential fatigue failure in this area can be attributed to a combination of coarse phase particle and grains, dissolution of phase particles leading to free precipitate zone and lower dislocation density in this region and a high rate of pitting corrosion at the interface between the weld metal and the heat-affected zone. As shown in

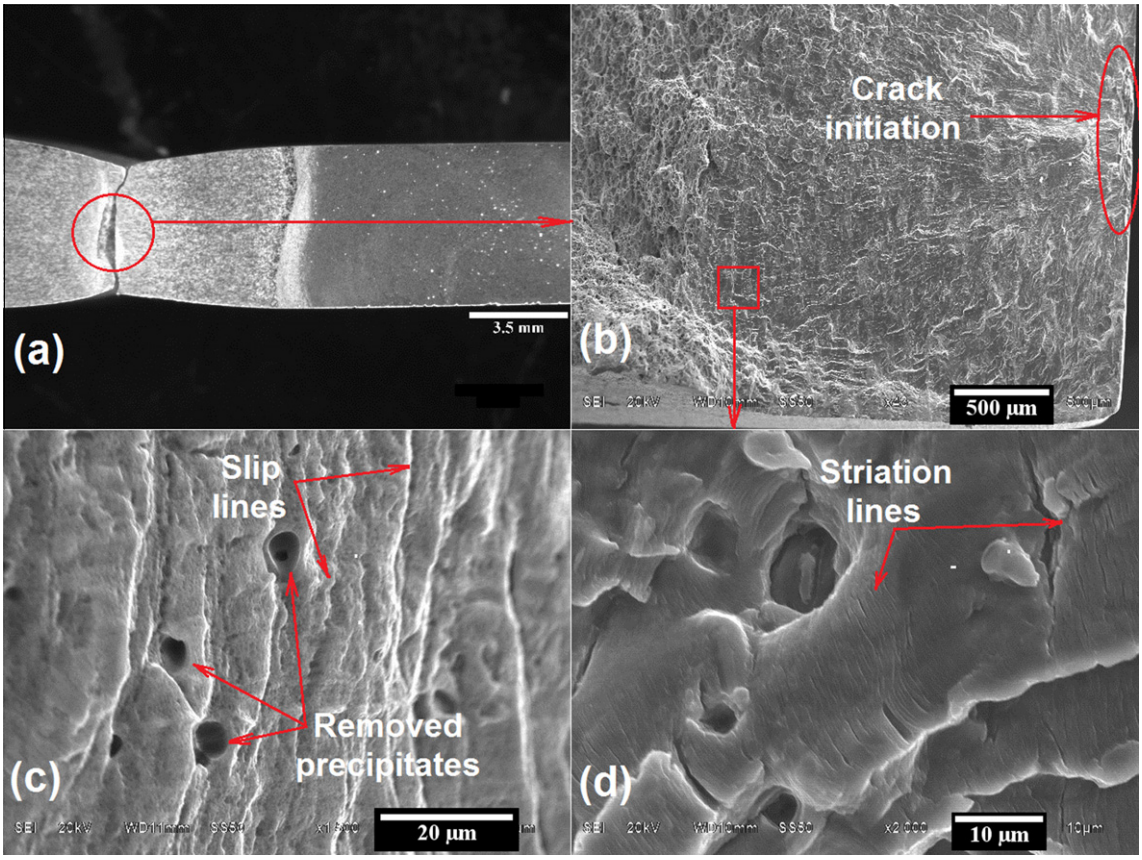

Fig. 8. Fatigue failure of aluminium 6061-T651 welded with ER5183 filler wire tested in ambient air: (a) crack location in the heat-affected zone; (b) fatigue crack initiation site; (c) the fracture surface with removed precipitates; and (d) removed precipitates on the fracture surface.

Fig. 9a–c, pits apparently initiated at the free surface adjacent to coarse precipitates, resulting in rapid fatigue crack propagation from corrosion pits.

The coarse particles observed associated with corrosion pits on the fracture surface were examined using the EDS facility of a scanning electron microscope, and elemental maps were drawn up to show the distribution of iron, silicon, calcium, magnesium and aluminium in the region of a corrosion pit. As demonstrated by the elemental maps shown in Fig. 10, the particles were shown to be enriched in iron and silicon, and to contain magnesium and some aluminium, and are probably strengthening precipitates overaged as a result of the high temperatures experienced by the heat-affected zone adjacent to the fusion line during the weld thermal cycle. Due to a possible galvanic effect between the Al–Si–Mg–Fe precipitates and the aluminium-rich matrix, pitting occurred preferentially adjacent to these particles on exposure to the NaCl solution. The corrosion pits acted as stress raisers at the sample surface during fatigue testing, and promoted the nucleation of fatigue cracks.

The corrosion fatigue failure may be explain using the slip oxidation mechanism. The pitting corrosion and corrosion fatigue crack growth are promoted by the breaking-up of the protective oxide layer by a slip mechanism and the resolution of metal ions at the crack tip area. Cracks initiating from corrosion pits may grow by slip-oxidation mechanism during the corrosion fatigue cycle. The alternating fatigue stress could probably increase the amount of slip planes at the crack tip, resulting in ease break of the protective oxide layer. This is consistent with the observation made also by Maeng et al. [10].

The influence of stress amplitude on the fatigue damage ratio ($N_{f\ NaCl}/N_{f\ Air}$) is shown in Fig. 11 for unwelded 6061-T651 and welded 6061/ER5183. The damage ratio of both sample sets decreases with an increase in stress amplitude. This can be attributed to accelerated pitting corrosion by high stress levels, which negatively affects the fatigue properties. High stress levels in the weld are probably due to residual tensile stresses in the vicinity of the welds caused by thermal processing, subsequent specimen machining and weld. The strengthening precipitates, within the heat-affected zone, tend to partially dissolve and overage leading to the lower hardness of heat affected zone (under the influence of the weld thermal cycle). The heat-affected zones of the welds therefore become preferential pitting corrosion sites (due to the galvanic effect between the coarse intermetallic particles and the matrix). The presence of corrosion pits associated with overaged precipitates and the low hardness of the heat-affected zone promote rapid fatigue crack nucleation and growth.

Unwelded 6061-T651 appears to be more resistant to corrosion fatigue in NaCl solution since the pitting corrosion rate is lower in this matrix.

4. Conclusions

The fatigue life of 6061-T651 aluminium in the unwelded condition is significantly reduced on testing in a 3.5% NaCl solution, compared to that measured in ambient air. This can be attributed to the incidence of pitting corrosion during testing in a NaCl solution. These corrosion pits appear to be associated with precipitates in the aluminium matrix and act as preferential fatigue crack initiation sites. This reduces the time required for fatigue crack initiation and decreases the total fatigue life.

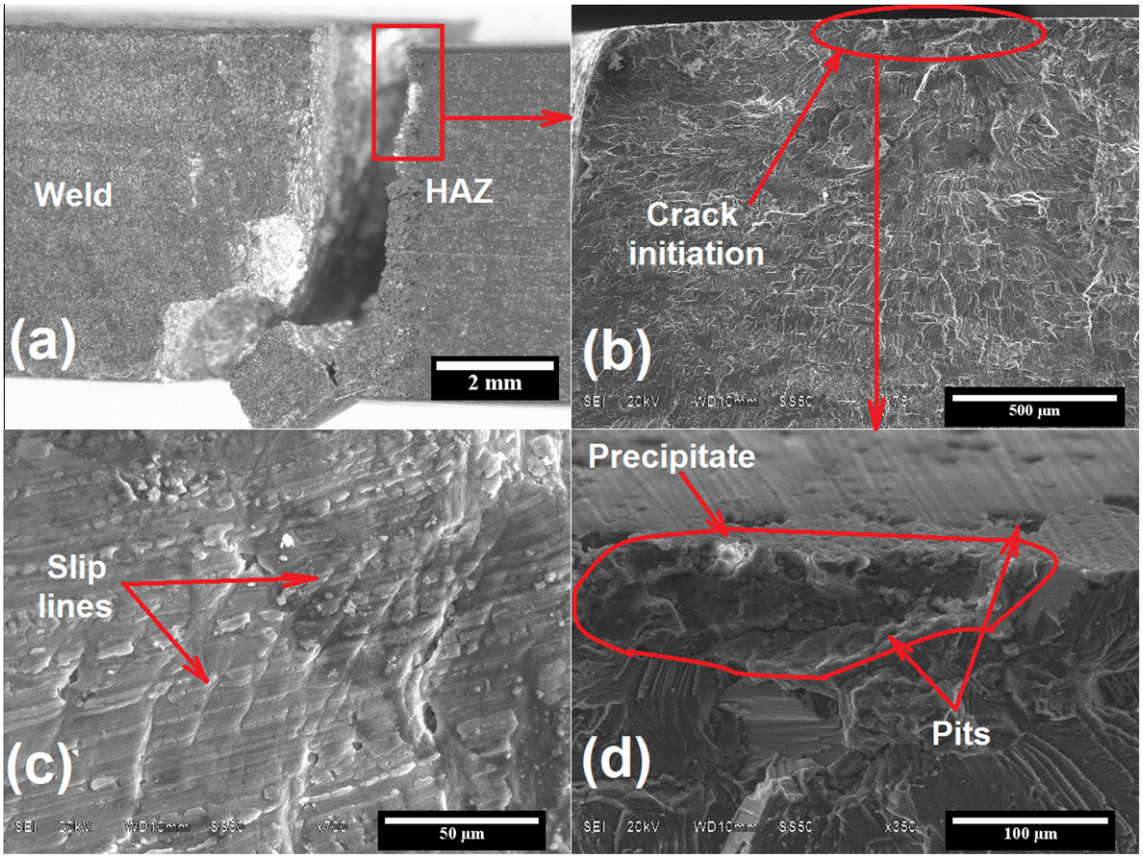

Fig. 9. Fatigue failure of aluminium 6061-T651 welded with ER5183 filler wire tested in a 3.5% NaCl solution: (a) crack location at the interface between the weld metal and heat-affected zone; (b) fatigue crack initiation site; (c) the fracture surface with precipitates; and (d) fatigue crack initiation associated with corrosion pits and precipitates.

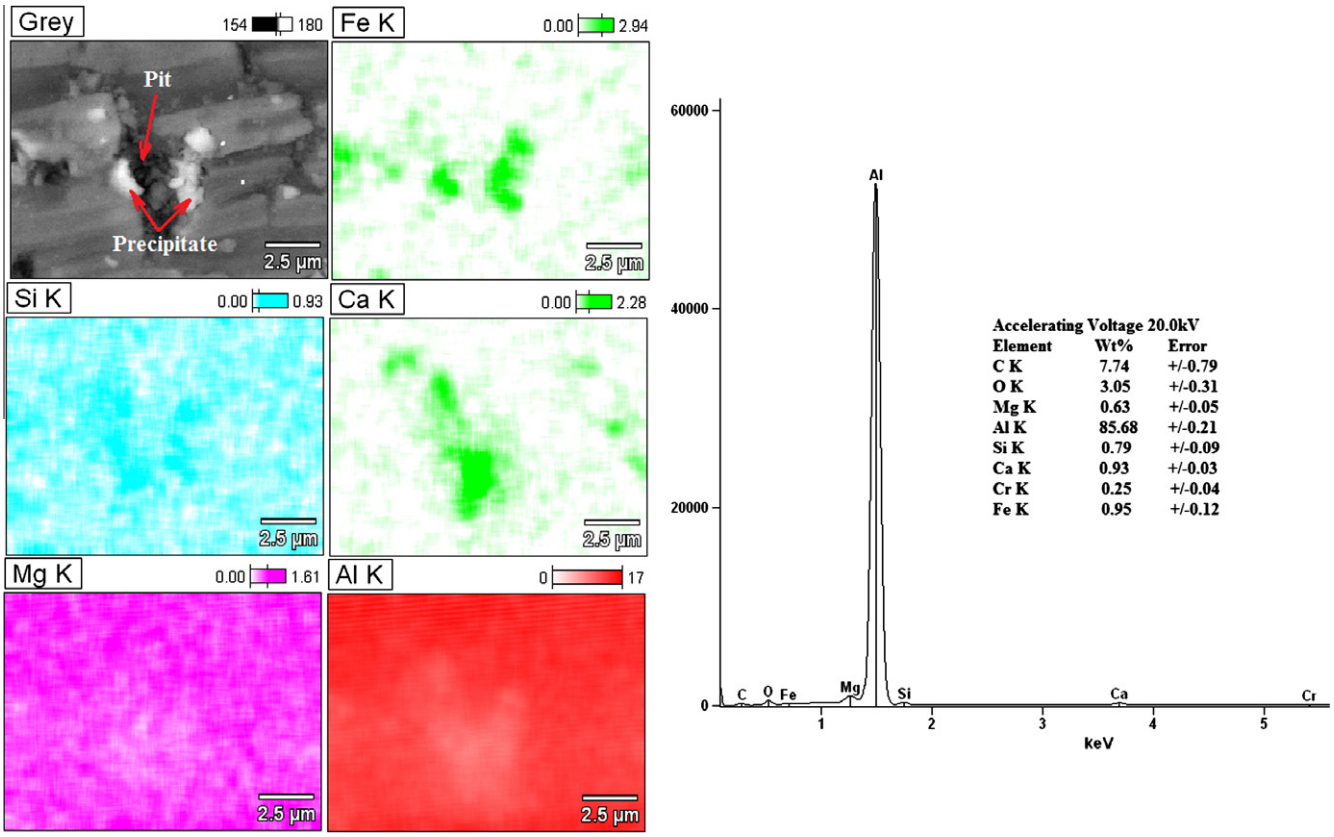

Fig. 10. EDS elemental maps showing the Fe, Si, Ca, Mg and Al distribution at the crack initiation site.

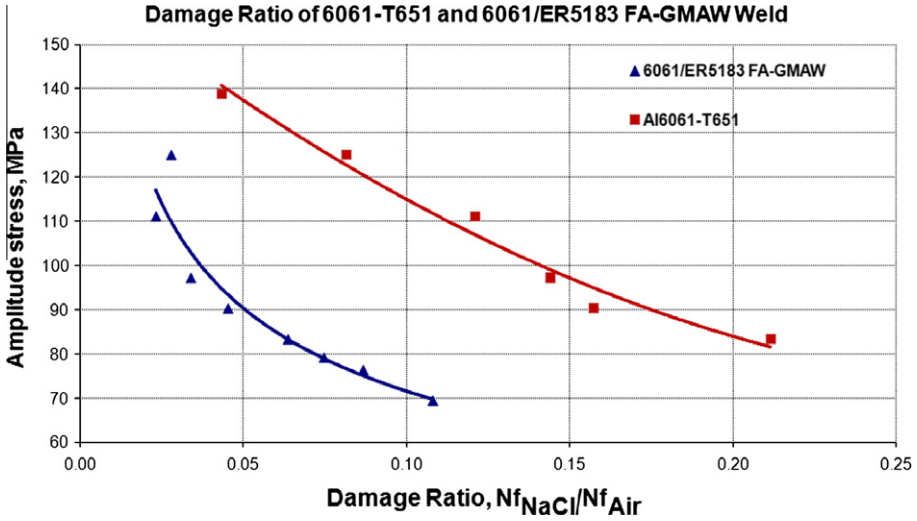

Fig. 11. Fatigue damage ratio ($N_{f\ NaCl}/N_{f\ Air}$) of aluminium 6061-T651 and 6061/ER5183 welds.

The fatigue life of 6061-T651 aluminium in the welded condition (welded using fully automatic gas metal arc welding with ER5183 filler wire) was considerably reduced in air and 3.5% NaCl solution. Since the fatigue samples were dressed and polished prior to testing (negating the effect of the weld toe geometry), the reduction in fatigue life in air appears to be associated with heterogeneous structure and high degree of heat-affected zone softening. On testing in a NaCl solution, the fatigue life was reduced even further. Pits formed preferentially at large second phase particles at the interface between the weld metal and heat-affected zone, and together with the coarse phase particles and grains in this region, facilitated rapid fatigue failure of the welded specimens.

Acknowledgements

The authors wish to thank the Light Metals Development Network, AFSA (Aluminium Federation of South Africa), the University of Pretoria and the CSIR (Council for Scientific and Industrial Research) for their fundamental contribution.

References

[1] Aydın H, Bayram A, Durgun I. The effect of post-weld heat treatment on the mechanical properties of 2024-T4 friction stir-welded joints. Mater Des 2010;31:2568–77.
[2] Elangovan K, Balasubramanian V. Influences of post-weld heat treatment on tensile properties of friction stir-welded AA6061 aluminum alloy joints. Mater Charact 2008;59:1168–77.
[3] Balasubramanian V, Ravisankar V, Reddy GM. Influences of pulsed current welding and post weld aging treatment on fatigue crack growth behaviour of AA7075 aluminium alloy joints. Int. J. Fatigue 2008;30:405–16.
[4] Balasubramanian V, Ravisankar V, Reddy GM. Effect of pulsed current and post weld aging treatment on tensile properties of argon arc welded high strength aluminium alloy. Mater Sci Eng 2007;459:19–34.
[5] Ahlatci H. Production and corrosion behaviours of the Al–12 Si–X Mg alloys containing in situ Mg_2 Si particles. J Alloys Compd, vol. In Press, Accepted Manuscript, no. 2010.04.214.
[6] Guillaumin V, Mankowski G. Localized corrosion of 6056 T6 aluminium alloy in chloride media. Corros Sci 2000;42:105–25.
[7] Chlistovsky RM, Heffernan PJ, DuQuesnay DL. Corrosion-fatigue behaviour of 7075-T651 aluminum alloy subjected to periodic overloads. Int J Fatigue 2007;29:1941–9.
[8] Rebiere M, Magnin T. Corrosion fatigue mechanisms of an 8090 AlLiCu alloy. Mater Sci Eng 1990;128:99–106.
[9] Rokhlin SI, Kim J, Nagy H, Zoofan B. Effect of pitting corrosion on fatigue crack initiation and fatigue life. Eng Fract Mech 1999;62:425–44.
[10] Maeng WY, Kang YH, Nam TW, Ohashi S, Ishihara T. Synergistic interaction of fatigue and stress corrosion on the corrosion fatigue crack growth behavior in alloy 600 in high temperature and high pressure water. J Nucl Mater 1999;275:194–200.
[11] ASTM International 2001. Standard guide for metallographic specimens, 2001st ed. West Conshohocken: ASTM International.
[12] ASTM International 2002. Standard test method for macroetching metals and alloys, 2002nd ed. West Conshohocken: ASTM International.
[13] Mutombo K, Du Toit M. Mechanical properties of 5083 aluminium welds after manual and automatic pulsed gas metal arc welding using E5356 filler. Mater Sci Forum 2010;654(656):2560–3.
[14] ASTM International 2004. Standard test method for Vickers hardness of metallic of materials, 2004th ed. West Conshohocken: ASTM international.
[15] ASTM International 2002. Standard practice for conducting force controlled constant amplitude axial fatigue test of metallic materials, 2002nd ed. West Conshohocken: ASTM International.
[16] ASTM International 2004. Standard practice for verification of constant amplitude dynamic forces in an axial fatigue testing system, 2004th ed. West Conshohocken: ASTM International.